

# Hybrid-Emba3D: Geometry-Aware and Cross-Path Feature Hybrid Enhanced State Space Model for Point Cloud Classification

Bin Liu<sup>a</sup>, Chunyang Wang<sup>a,b,\*</sup>, Xuelian Liu<sup>a</sup>, Guan Xi<sup>a</sup>, Ge Zhang<sup>a</sup>, Ziteng Yao<sup>a</sup>, Mengxue Dong<sup>a</sup>

<sup>a</sup>*Xi'an Technological University, Xi'an, 710021, Shaanxi, China*

<sup>b</sup>*Changchun University of Science and Technology, Changchun, 130022, Jilin, China*

---

## Abstract

The point cloud classification tasks face the dual challenge of efficiently extracting local geometric features while maintaining model complexity. The Mamba architecture utilizes the linear complexity advantage of state space models (SSMs) to overcome the computational bottleneck of Transformers while balancing global modeling capabilities. However, the inherent contradiction between its unidirectional dependency and the unordered nature of point clouds impedes modeling spatial correlation in local neighborhoods, thus constraining geometric feature extraction. This paper proposes Hybrid-Emba3D, a bidirectional Mamba model enhanced by geometry-feature coupling and cross-path feature hybridization. The Local geometric pooling with geometry-feature coupling mechanism significantly enhances local feature discriminative power via coordinated propagation and dynamic aggregation of geometric information between local center points and their neighborhoods, without introducing additional parameters. The designed Collaborative feature enhancer adopts dual-path hybridization, effectively handling local mutations and sparse key signals, breaking through the limitations of traditional SSM long-range modeling. Experimental results demonstrate that the proposed model achieves a new SOTA classification accuracy of 95.99% on ModelNet40 with only 0.03M additional. Our code and weights are available at <https://github.com/L1277471578/Hybrid-Emba3D>.

*Keywords:* State Space Model, Point Cloud, Classification, Local geometry

---

## 1. Introduction

Point clouds directly represent the geometric features of objects through 3D coordinates, compensating for the lack of spatial information in 2D data and providing basic data support for perception tasks such as 3D object recognition and scene understanding[19]. However, the inherently disordered nature of point cloud data necessitates permutation invariant processing, and effective extraction of local geometric features is constrained by nonuniform distribution, these intrinsic characteristics present challenges for improving the accuracy and generalization capability of 3D point cloud classification models.

In response to the challenges of point cloud disorder and local feature extraction, researchers have explored. Among them, PointNet[4] innovatively integrates multi-layer perceptrons and symmetric functions, and builds a processing framework with permutation invariance for the first time, laying the foundation for the direct representation of the disordered features of point clouds. Subsequent research further captures local geometric features by developing point cloud convolution operations[44, 20, 47]. However, the convolution-based method is essentially local feature aggregation, which makes it difficult to model the long-distance dependency in point cloud data and limits its performance improvement in complex scenes. Some researchers have shifted their focus to Transformer[38] archi-

tectures with global modeling capabilities to overcome the limitations of the convolution method.

The PointTransformer[8] pioneered the application of self-attention mechanisms in 3D point cloud processing, utilizing positional encoding and multi-head attention mechanisms to establish comprehensive modeling of global dependencies within point clouds. While subsequent studies have enhanced feature representation capabilities through refined local regional modeling and hierarchical architectural designs, the intrinsic quadratic computational complexity of Transformer-based frameworks persistently suffers from dual constraints on computational resources and inference speed[18].

State Space Model (SSM) is an emerging sequence modeling method in the field of deep learning. It realizes efficient long sequence modeling with the mathematical characteristics of continuous state representation and linear time-invariant systems. By introducing a selective mechanism with input dependency, the Mamba model[11] innovatively constructs a state space architecture with conditional computing characteristics. It combines the timing dependence modeling capabilities of RNNs[22] with the parallel computing advantages of the Transformer to achieve linear time complexity of long-distance dependence modeling. However, the irregular topological characteristics of point cloud data make it difficult for the SSM discrete state transfer mechanism to effectively capture geometric correlations. Furthermore, SSM's unidirectional scanning paradigm is inadequate in modeling the intrinsically bidirectional spatial dependencies embedded within point clouds, par-

---

\*corresponding author

ticularly in local feature refinement processes where this limitation inevitably induces structural information loss of geometric details.

To address these limitations, this paper proposes a Geometry-Aware and Cross-Path Feature Hybrid Enhanced Mamba Model (Hybrid-Emba3D), which realizes lightweight local spatial information feature enhancement and feature cross-path fusion, improving the ability to extract local and global information.

The main contributions of this work can be summarized as follows:

- A lightweight feature coupling mechanism based on geometric priors is proposed, which couples geometric feature information between center point features and neighboring point spatial geometric information, enriching local geometric representations.
- Designing a multi-dimensional hybrid feature enhancement module with channel-wise and multi-scale learning capabilities, which enhances context-aware modeling capacity for SSM.
- The proposed model demonstrates exceptional performance, particularly outperforming existing SOTA models on the ModelNet40 benchmark and establishing new performance benchmarks. As shown in Figure 1.

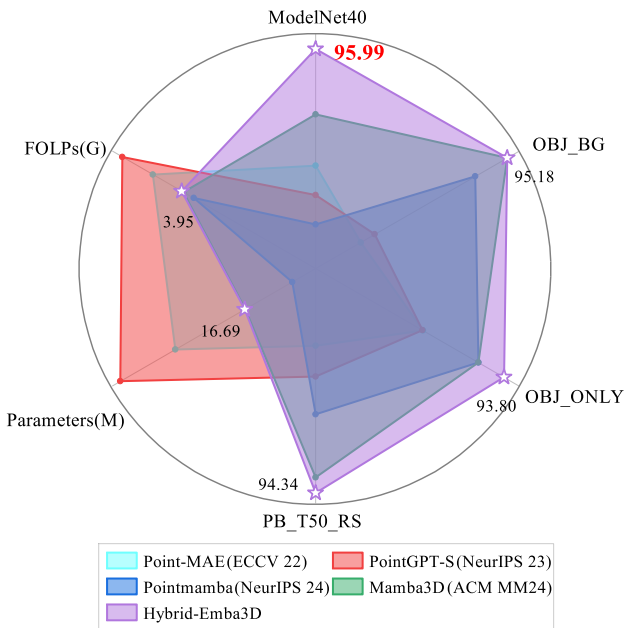


Figure 1: Comprehensive comparison of Hybrid-Emba3D with other SOTA models

## 2. Related work

### 2.1. Deep learning for point cloud data

Effective point cloud classification requires the collaborative modeling of local geometric details and global spatial

context. Maturana[29] et al. proposed VoxNet, which organizes unstructured point clouds into 3D voxel grids and applies conventional 3D convolutional neural networks to capture comprehensive spatial contextual features. Based on PointNet, PointNet++[31] employs Farthest Point Sampling (FPS) to construct hierarchical architectures while enhancing localized detail extraction through its local feature aggregation mechanism. Its density-adaptive modules effectively mitigate multi-scale learning interference caused by non-uniform point density distributions. Subsequent approaches encompass point-based direct convolution[36, 26, 9, 42], Volume-Based convolution [34, 35, 17, 43], and graph-based convolution[41, 28, 40, 24]. They are all attempts to enhance local feature extraction through spatial transformations or deformable convolutional kernels. However, these methodologies fundamentally suffer from the mismatch between fixed receptive fields and irregular point distributions.

In 2021, PointTransformer[8] was the first to introduce the Transformer architecture, marking a new stage in global context modeling for point cloud processing. Based on relative position coding, its self-attention mechanism can adaptively establish geometric correlations between point cloud elements and significantly improve the scene semantic understanding ability through global dependency modeling[30, 48, 51, 14, 45]. Notably, the architecture’s intrinsic permutation equivariance naturally conforms with the unordered nature of point clouds, eliminating the need for data rearrangement or interpolation required by voxel/grid-based methods, thereby avoiding the information loss caused by three-dimensional coordinate discretization.

The conflict exists between the sparse distribution characteristics of point cloud data and the dense connectivity assumption underlying standard attention mechanisms, leading to redundant attention weight allocations. Researchers have developed sparse attention strategies to improve this. Such as DSVT[10] with hierarchical feature aggregation demonstrates optimized computation-accuracy balance through adaptive sparse attention patterns; Point-BERT[48] self-supervised pretraining via masked point modeling, effectively reducing annotation dependency; PatchFormer[50] significantly reduces computational complexity through geometrically consistent patch partitioning and streamlined patch-level attention mechanisms.

While convolution-based architectures exhibit linear computational complexity, their localized receptive fields fundamentally constrain long-range contextual modeling capabilities. Conversely, Transformer models achieve global interaction through self-attention mechanisms, yet are inherently limited by quadratic computational complexity. In this context, state space models (SSMs) like Mamba demonstrate potential for point cloud processing, achieving linear modeling characteristics in long-sequence modeling that significantly reduce both computational and spatial overhead while preserving global dependency learning.

### 2.2. State Space Model

SSM, a classic method in control theory, achieves dynamic system modeling by constructing the state space. As control

theory evolved, the limitations of traditional input-output models have gradually emerged. SSM establishes a system state space based on input signal characteristic variables, uses state variables to characterize the dynamic evolution of the system fully, and abstracts the system into a mathematical model containing state and output equations. The SSM structure are shown in Figure 2.

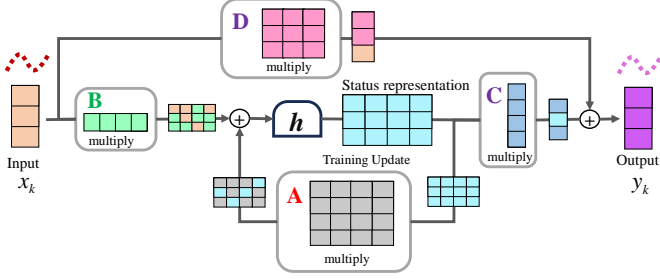


Figure 2: Mamba block and SSM structure

Discretize the continuous-time linear time-invariant (LTI) state space model using the zero-order hold (ZOH) method. The discretized equation of state is given in equation 1.

$$\begin{cases} h_k = \bar{A} \cdot h_{k-1} + \bar{B} \cdot x_k \\ y_k = \bar{C} \cdot h_k + \bar{D} \cdot x_k \end{cases} \quad (1)$$

Where:  $\bar{A}$  is a discrete state transition matrix,  $\bar{B}$  is a discrete control input matrix,  $\bar{C}$  is a discrete observation matrix, and  $\bar{D}$  is a discrete feedforward matrix.  $h_k$  is the current state variable,  $h_{k-1}$  represents the hidden state of the system at the discrete time point  $k-1$ , containing historical information up to that time, and  $k$  is the discrete time step index.

Traditional SSMs[12, 13, 2] employ static predefined parameters for matrices  $\bar{A}$ ,  $\bar{B}$ , and  $\bar{C}$ , resulting in rigid information propagation pathways. In contrast, Mamba’s SSM[11] layer implements a selective mechanism that dynamically generates timestep-specific parameters  $\Delta$  conditioned on input data. This enables adaptive modulation of the discretization processes for B and C matrices, thereby establishing context-sensitive information propagation paths. Generate parameters  $\Delta$ ,  $\bar{B}$ ,  $\bar{C}$  in real time from the input sequence through linear transformation:

$$B_k = \text{Linear}_B(x_k) \in \mathbb{R}^{N \times 1} \quad (2)$$

$$C_k = \text{Linear}_C(x_k) \in \mathbb{R}^{N \times 1} \quad (3)$$

$$\Delta_k = \text{softplus}(\text{Linear}_\Delta(x_k)) \in \mathbb{R}^+ \quad (4)$$

Where: Linear represents linear projection, and  $\Delta$  is the step length at which ZOH discretizes the continuous equation.

Dynamically adjust the discretization process according to the input:

$$\bar{A}_k = \exp(\Delta_k A_k) \quad (5)$$

$$\bar{B}_k = (\Delta_k A_k)^{-1} (\exp(\Delta_k A_k) - I) \Delta_k B_k \quad (6)$$

$$\bar{C}_k = C_k \quad (7)$$

Plugging parameter  $\bar{A}$ ,  $\bar{B}$ ,  $\bar{C}$  into Equation 1, the selective SSM still follows the LTI property in the continuous time

domain, thus allowing efficient GPU-accelerated convolution computing of the discretized state space equation:

$$\bar{K} = (\overline{C_k B_k}, \overline{C_k A_k B_k}, \dots, \overline{C_k A_k^{L-1} B_k}) \quad (8)$$

$$y_k = x_k * \bar{K} \quad (9)$$

Where:  $\bar{K}$  is the global convolution kernel,  $L$  is the length of the convolution kernel.

In summary, the selective SSM’s continuous-time equation is formally consistent with traditional SSM, but content-aware modeling is realized through the dynamic parameterization of the discretization process. This design paradigm transcends LTI limitations while inheriting the theory of continuous systems, enabling Mamba to simultaneously attain computational efficiency comparable to RNNs ( $O(n)$  complexity) and expressive power equivalent to Transformer architectures.

PointMamba[21] pioneers the introduction of Mamba architecture into point cloud processing, which significantly improves efficiency while maintaining high accuracy, demonstrating the potential of Mamba in 3D vision tasks.

### 3. Hybrid-Emba3D

While Mamba achieves input-dependent parameter adaptation through selective gating mechanisms, its core architecture remains anchored in RNN-style sequential recurrence. This design introduces inherent constraints in global context sensitivity during long-range dependency modeling, potentially limiting the comprehensive capture of complex interaction patterns.

#### 3.1. Overview

This work establishes a hybrid framework that effectively enhances the representation performance of the Mamba. It integrates the Local geometric pooling (LGP) with geometric feature coupling and a bidirectional SSM enhanced by the collaborative feature enhancer (CoFE-BiSSM). The architecture of the model is shown in Figure 3.

Given an input point cloud  $P \in \mathbb{R}^{N \times 3}$  with  $N$  points, the framework first initializes  $L$  centroid points via Farthest Point Sampling (FPS) to form a set  $P_{\text{center}} \in \mathbb{R}^{L \times 3}$ . For each centroid  $P_{\text{center}}$ , the method retrieves its  $K$ -Nearest Neighbors (KNN) from the original cloud to construct local patches  $x_p^i \in \mathbb{R}^{K \times 3}$  serving as structural spatial primitives. A lightweight PointNet variant subsequently performs hierarchical feature encoding on each patch, with the resultant local descriptors simultaneously serving as input token sequences for Hybrid-Emba3D architectures.

Adhering to the ViT’s[7] work, the architecture embeds a learnable [class] token preceding  $L$  local tokens for global representation aggregation. Each patch  $x_p \in \mathbb{R}^{L \times K \times 3}$  is projected and mapped into a  $C$ -dimensional feature vector  $W_{\text{patch}}(x_p) \in \mathbb{R}^{L \times C}$  as its initial patch embeddings. The [class] token is vertically stacked with all point cloud block features, forming a sequence matrix with a shape of  $(L+1) \times C$  ( $L$  patch features + one [class]). After superimposing position encoding  $P_{\text{pos}}$ , the geometric structure information of the original point cloud is

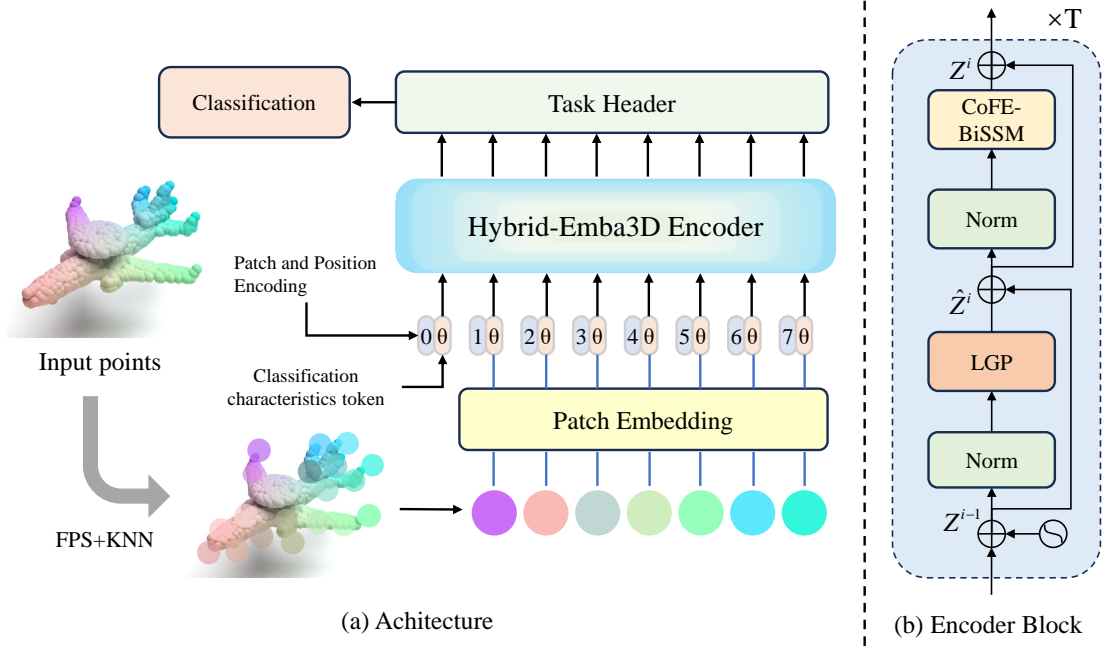


Figure 3: The architecture of Hybrid-Emba3D. The input point cloud is sampled into local patches via FPS and KNN, and the coordinates and features are aggregated into embedding vectors through lightweight PointNet. After incorporating positional encoding and classification tokens, input the Hybrid-Emba3D encoder. The encoder core is composed of alternately stacked CoFE-BiSSM and LGP, supplemented by normalization and residual connections. Task-specific heads finally decode the transformed features for the classification of objects.

preserved through patch position encoding, providing an initial representation for subsequent hierarchical encoding.

$$Z^0 = [x_{cls} + P_{pos}^{(0)}, W_{patch}(x_p^1) + P_{pos}^{(1)}, \dots, W_{patch}(x_p^L) + P_{pos}^{(L)}] \quad (10)$$

Where:  $Z^0$  is the initial input layer feature,  $x_{cls} \in \mathbb{R}^{1 \times C}$  is the [class] token,  $W_{patch}(x_p^1), W_{patch}(x_p^2) \dots, W_{patch}(x_p^L)$  is the concatenated point cloud patch feature processed by the lightweight PointNet variant ( $W_{patch}$ ), and  $P_{pos}$  is the positional encoding.

The encoder employs dual-phase processing (The encoder block is shown in Figure 3 (b)): For the  $i$ -th layer, input features  $Z^{i-1}$  undergo normalization before the LGP component executes geometry-aware local feature extraction to generate  $\hat{Z}^i$ . Post residual summation, secondary normalization precedes the CoFE-BiSSM component, which supplants conventional attention mechanisms, enabling dynamic feature enhancement and long-range dependency capture, ultimately outputting the current layer representation  $Z^i$ . The overall structure retains the residual connection. The process is as follows:

$$\hat{Z}^i = \text{LGP}(\text{Norm}(Z^{i-1} + P_{pos})) + Z^{i-1}, \quad (11)$$

$$Z^i = \text{CoFE-BiSSM}(\text{Norm}(\hat{Z}^i)) + \hat{Z}^i \quad (12)$$

The architecture employs task-specific heads (e.g., classification MLPs) for diverse downstream tasks, while integrating learnable positional embeddings within each encoder layer to enhance spatial awareness. This structure ingeniously transplants the achievements of the Transformer into the Mamba series.

### 3.2. Local geometric pooling with geometry-feature coupling mechanism

Local features are crucial for point cloud feature learning. The local features in point clouds are usually obtained by constructing a local domain using KNN and then performing feature fusion. Mamba3D simplifies local feature extraction to feature propagation and aggregation operations, but ignores the spatial geometric information of local neighborhoods. Therefore, we have designed a local geometry-feature coupling mechanism, which mainly contains local feature normalization, local geometry patch normalization, and feature coupling operations.

According to Section 3.1 and Figure 4,  $L$  local domains with  $k$  neighbors are constructed using KNN around each center point. The center point of these local domains is  $P_{center} \in \mathbb{R}^{L \times 3}$ , and the coordinates of the neighborhood point are  $k_i$ .

For the local feature normalization, given the center point feature and its  $K$  nearest neighbor feature  $\tilde{F}_K \in \mathbb{R}^{L \times K \times C}$ , the relative feature offset  $\Delta F = F_K - F_C$  is first calculated and channel normalized:

$$\tilde{F}_K = \frac{\Delta F}{\sqrt{\text{Var}(\Delta F) + \varepsilon}} \quad (13)$$

The normalized neighbor features and the center point features are concatenated along the channel, and the propagation features can be generated through learning an affine transformation:

$$\hat{F}_K \in \mathbb{R}^{L \times K \times 2C} = \text{Concat}(\tilde{F}_K, F_C) \odot \gamma + \beta \quad (14)$$

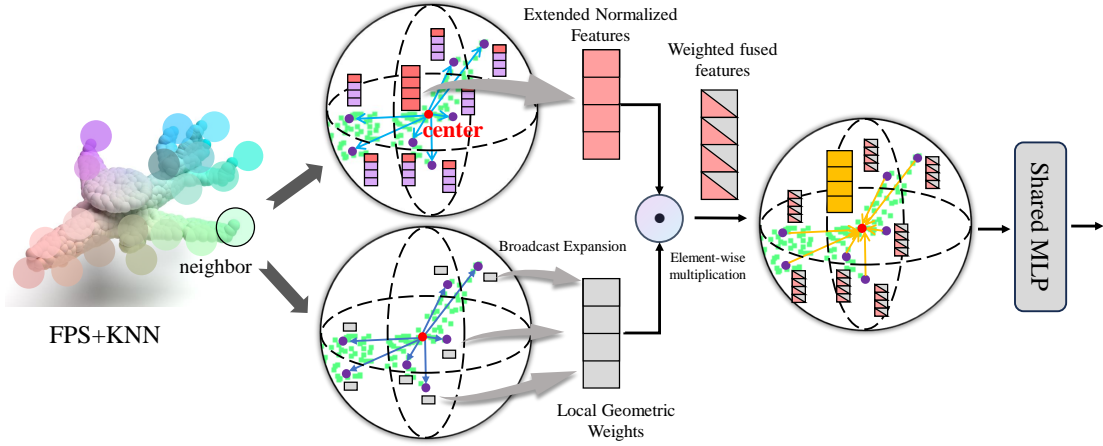


Figure 4: Illustration of LGP. This process selects neighboring points through FPS and KNN, extracts normalized features from the center points, and element-wise multiplication with the broadcast extended local geometric weights to achieve the fusion of features and geometric information, followed by a shared MLP for advanced feature extraction.

Where:  $\gamma$  and  $\beta$  are trainable proportional coefficients and shift vectors, respectively.

That implements feature-aware adaptive updates by explicitly encoding the center-neighborhood feature relationship.

For the local geometric patch normalization, firstly compute the mean coordinate  $\mu$  of  $M$  points within the patch, then convert the coordinates of each point into offsets  $\Delta p = p_j - \mu$  relative to the patch centroid to eliminate global translational effects. Subsequently, calculate the coordinate standard deviation  $\sigma = \sqrt{\sum_{x=1}^M \|\Delta p_j\|_2^2 + \varepsilon/M}$ , and normalize the coordinates by  $p'_j = \Delta p_j / \sigma$  to eliminate local scale differences. This process ensures that the geometric encoding achieves translation-scale invariance. The process can be formalized as:

$$p'_j = \frac{p_j - \mu}{\sqrt{\frac{1}{M} \sum_{k=1}^M \|p_k - \mu\|_2^2 + \varepsilon}} \quad (15)$$

Where:  $p_j, p_k \in \mathbb{R}^3$  are 3D coordinates of the  $j$ -th or  $k$ -th point in the local geometric patch;  $\mu$  is the Centroid of the geometric patch,  $\mu = \sum_{k=1}^N p_k / M$ ;  $j, k$  are point indices, where  $j$  is used for calculating the offset of individual points, and  $k$  is used for summation traversal over all points;  $\varepsilon$  is the numerical stability term.

This standardization operation enables local geometric features to have translation invariance and scale invariance, significantly improving the model's generalization ability to geometric deformations. Furthermore, Gaussian spatial weights are constructed based on the Euclidean distances between each point in the local patch and the center point to model the geometric structure correlation:

$$\Delta p_i = p_i - p_c, \quad (16)$$

$$w_i = \exp(-\|\Delta p_i\|_2), \quad (17)$$

$$W = \text{Broadcast}(w_i) \in \mathbb{R}^{2C \times L \times K} \quad (18)$$

$$F_{\text{weighted}} = \hat{F}_k \odot W \quad (19)$$

Where:  $p_i, p_c \in \mathbb{R}^3$  represent the coordinates of patch points and the center point;  $w_i \in \mathbb{R}^{L \times K \times 1}$  is a weight coefficient based on distance attenuation,  $\hat{F}_k$  is a normalized feature tensor, with a shape of  $2C \times L \times K$ ;  $\odot$  represents element-wise multiplication;  $\text{Broadcast}(\cdot)$  extends the weight vector to align with the feature dimension.

The final feature  $F_{\text{agg}} \in \mathbb{R}^{2C \times L}$  is obtained using the Softmax weighted average to achieve adaptive aggregation of neighborhood features:

$$F_{\text{agg}} = \frac{\sum_{k=1}^K F_{\text{weighted}} \cdot \exp(F_{\text{weighted}})}{\sum_{k=1}^K \exp(F_{\text{weighted}})} \quad (20)$$

Finally, channel alignment is completed through the shared MLP.

This component constructs parameter-free geometric weights using Gaussian kernel functions, leveraging distance-dependent decay characteristics between points to reinforce local structural awareness. These weights exhibit well-defined physical significance, being solely geometry-driven without extra parameters. Through a coupling mechanism between spatial distribution and feature representation, it effectively enhances sensitivity to local structures.

### 3.3. Bidirectional SSM with the Collaborative feature enhancer

While Mamba achieves theoretical benefits in long-sequence modeling through SSMs, its RNN-based recurrent architecture inherently suffers from constrained effective receptive fields due to error accumulation in sequential processing, exhibiting a deficiency in long-range dependency modeling efficiency compared to Transformer architectures.

The proposed Collaborative feature enhancer (CoFE) component adopts the dual-path architecture for long-range sequence modeling, enabling efficient global context capture via grouped multi-scale fusion. The structure is shown in Figure 5.

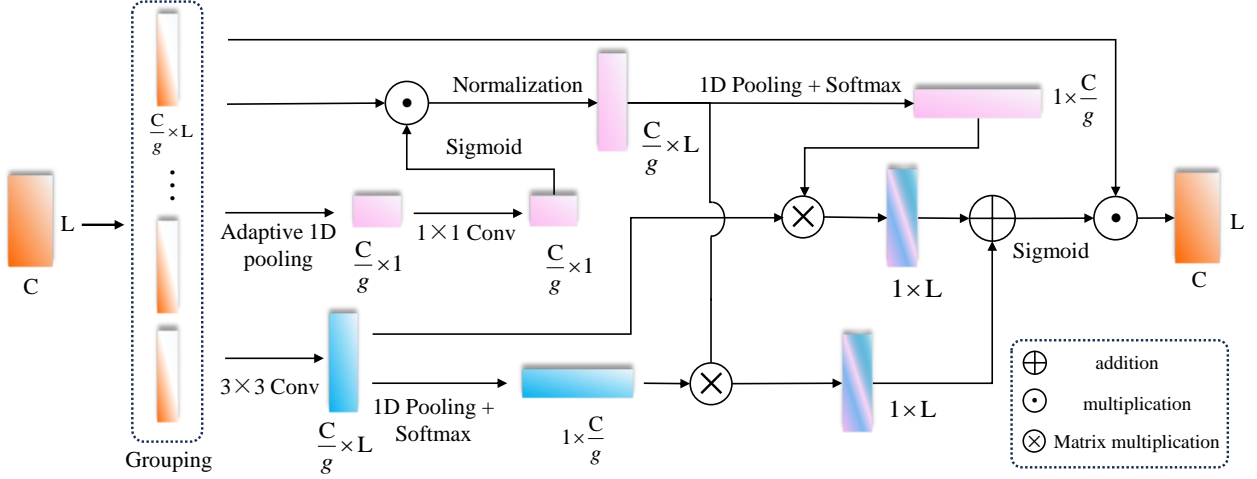


Figure 5: Details of Collaborative feature enhancer

Given the input tensor  $X \in \mathbb{R}^{B \times C \times L}$  divided into  $g$  groups along the channel dimension:

$$X' = \text{Reshape}(X, [B \cdot g, \frac{C}{g}, L]) \quad (21)$$

Construct parallel dual-path features—the  $3 \times 3$  convolutional path and the gated normalized path to extract local details and global context:

$$X_1 = GN(X' \odot \sigma(\text{Conv}_{1 \times 1}(P_{\text{Avg}}(X')))) \in \mathbb{R}^{(B \cdot g) \times \frac{C}{g} \times L} \quad (22)$$

$$X_2 = \text{Conv}_{3 \times 3}(X') \in \mathbb{R}^{(B \cdot g) \times \frac{C}{g} \times L} \quad (23)$$

Where:  $GN$  means GroupNorm normalization,  $P_{\text{avg}}$  is adaptive average pooling.

Perform cross-channel global feature compression on two paths, compress into a single channel, preserve information in the spatial dimension  $L$ , and serve as the basis for spatial attention weights:

$$\phi(X_i) = F_{\text{soft}}(P_{\text{avg}}(X_i)) \in \mathbb{R}^{(B \cdot g) \times \frac{C}{g} \times L} \quad (24)$$

Where:  $F_{\text{soft}}$  is the row-wise Softmax.

Subsequently, cross-path bidirectional interaction is performed to multiply the compressed feature matrices  $\phi(X_1)$  and  $\phi(X_2)$ :

$$X_1 \rightarrow X_2 : \phi(X_1)X_2 \in \mathbb{R}^{B \cdot g \times 1 \times L} \quad (25)$$

$$X_2 \rightarrow X_1 : \phi(X_2)X_1 \in \mathbb{R}^{B \cdot g \times 1 \times L} \quad (26)$$

The output at this time is a correlation matrix between spatial positions, which is used to characterize the degree of feature matching at different positions ( $L$  dimensions). The correlation matrix between spatial positions is normalized and activated by the gating mechanism to achieve nonlinear scaling of the normalized weights:

$$W = \sigma(\phi(X_1)X_2 + \phi(X_2)X_1) \quad (27)$$

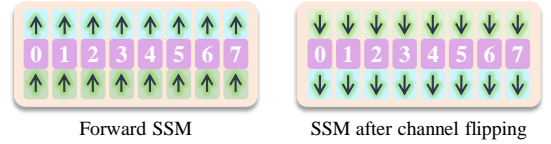
Where:  $\sigma(\cdot)$  is the Sigmoid.

Finally, merge the weights and adjust the output shape:

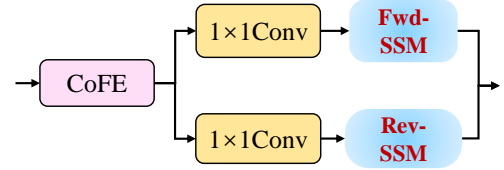
$$\text{output}' = X' \odot W \in \mathbb{R}^{(B \cdot g) \times \frac{C}{g} \times L} \quad (28)$$

$$\text{output} = \text{Reshape}(\text{output}', (B, C, L)) \quad (29)$$

CoFE employs dual pathways to capture local-global contexts, where a dynamic weight matrix explicitly fuses cross-scale features via bidirectional interaction ( $X_1 \rightleftharpoons X_2$ ). This interaction computes spatial affinities to eliminate unidirectional bias and adaptively models non-uniform dependencies in long sequences, delivering a lightweight attention enhancement for BiSSM (see Figure 6).



(a) Diagram of Forward and Reverse SSM



(b) CoFE-BiSSM

Figure 6: The structure of CoFE-BiSSM

The unidirectional nature of Mamba restricts global dependency capture in point cloud processing. Unlike Vision Mamba's[53] token-level horizontal flipping, a reverse path through vertical flipping of feature channels is constructed. The resulting BiSSM module is formulated as:

$$F' = \text{CoFE}(\text{Conv}_{1 \times 1}(F)) \quad (30)$$

$$\text{CoFE-BiSSM} = \text{Linear}(\text{FwdSSM}(F') + \text{RevSSM}(\text{Flip}_C(F'))) \quad (31)$$

Where:  $Flip_C(\cdot)$  is the Channel Flip operation.

This approach eliminates reliance on point cloud token order, enabling the model to focus on inherent distribution patterns of feature vectors rather than artificially constructed sequential orders. While Mamba’s core mechanism captures long-range dependencies through parameterized state transition equations, it demonstrates insufficient sensitivity to local transient features. The CoFE component complements the SSM framework by directly modeling inter-position relationships. The  $X_2$  pathway reduces the limitations of SSMs in capturing local details through localized context aggregation. Subsequent  $X_1 \rightleftharpoons X_2$  interaction facilitates complementary integration of feature correlation and provides more discriminative input to SSMs, enabling SSMs to dynamically perceive global contextual patterns while effectively modeling complex sequential dependencies.

## 4. Experiments

In this section, we first introduced hyperparameter settings and performance evaluation metrics. Secondly, conduct ablation experiments to evaluate the effectiveness of the components. Finally, the performance on target classification and small sample learning tasks was demonstrated.

### 4.1. Implementation Details

We conducted experiments under two distinct training protocols: training from scratch and fine-tuning. The cross-entropy loss function was adopted as the optimization objective for both settings. All experiments were performed on one NVIDIA TITAN RTX GPU without mixed-precision acceleration.

The model employs 12-layer encoders, feature dimension of 384. Point clouds are partitioned into 128 groups (Group Size=32) during preprocessing. Training uses AdamW optimizer with initial learning rate of  $5e-4$ , weight decay of 0.05, cosine scheduler (CosLR), drop path rate of 0.2, warmup epochs of 10, and batch size of 32 for 300 epochs. This experiment employs overall accuracy (OA) as the classification performance indicator. Parameters quantify model complexity, and FLOPs measure computational complexity.

### 4.2. Object classification

**Datasets:** ModelNet40[46], a widely adopted benchmark dataset for 3D point cloud processing, comprises 12,311 structurally aligned 3D CAD models spanning 40 common object categories. ScanObjectNN[37], a real-world 3D object classification dataset, includes three variants: OBJ\_BG (with Background), OBJ\_ONLY (Vanilla), and PB\_T50\_RS (Perturbed with 50% Translation, Rotation, and Scaling). These variants respectively simulate practical challenges, with PB\_T50\_RS being the most challenging variant. The dataset contains ~15K objects across 15 indoor object categories.

**Training Settings:** For fine-tuning, the pre-training employs the Point-MAE framework with masked self-supervised learning on the ShapeNetCore[3] dataset. Unless explicitly specified, consistent training parameters are maintained between scratch training and fine-tuning. The Hybrid-Emba3D

classification task header utilizes a 3-layer MLP classifier ( $256 \rightarrow 256 \rightarrow C$  channels). In the ModelNet40 experiment, adopting the standard division (9843 train/2468 test), sampling 1024 points, and using scale&translation augmentation, while ScanObjectNN followed the original train/test split, sampling 2048 points, and using the rotation augmentation. The experimental results are shown in Table 1.

**Comparison with existing SOTA methods:** Hybrid-Emba3D achieves SOTA performance across multiple benchmarks. Without pretraining, the model attains 94.0% accuracy on ModelNet40, surpassing the comparable Mamba3D by 0.6%, while achieving the highest OBJ\_BG accuracy of 93.63%. When employing Point-MAE pretraining, Hybrid-Emba3D breaks the 95.58% accuracy barrier on ModelNet40, further reaching 95.99% with the voting strategy, establishing a new record for this benchmark. Hybrid-Emba3D outperforms SOTA Transformer counterparts (PointGPT-S, Point-FMAE) by 1.99% and 0.84% in accuracy, while reducing Parameters by 41.9% and 39.1%, respectively. Compared to similar Mamba-based models (Pointmamba, Mamba3D), it achieves 0.89% and 1.0% accuracy gains on ModelNet40 and ScanObjectNN-PB\_T50\_RS (the most challenging benchmark) with only exchanged 0.06M Parameters and 0.05G FLOPs.

**Feature visualization:** High-dimensional features are reduced via t-SNE to a 2D projection distribution to visualize the clustering effect of features. As shown in Figure 7. On ModelNet40, the feature distribution is relatively scattered, and there are ambiguous inter-class boundaries, indicating that the Hybrid Emba3D needs to improve its ability to distinguish specific categories. While OBJ\_BG and PB\_T50\_RS demonstrate prominent clustering tendencies with minor inter-class overlaps, OBJ\_ONLY achieves superior class separation. The model maintains robust clustering performance under PB\_T50\_RS interference scenarios, confirming its resilience to environmental disturbances.

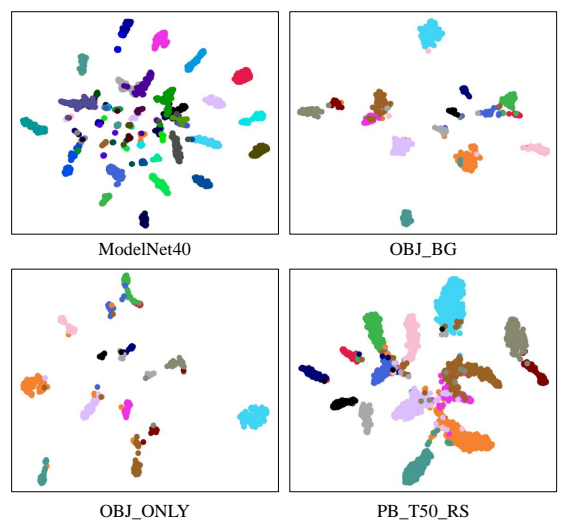


Figure 7: Details of Collaborative feature enhancer

**Analysis of analysis category confusion:** Overall performance is good on ModelNet40 (see Table 1 and Figure 8), but

Table 1: Experimental results of ModelNet40 and ScanObjectNN. Compared with methods of different architectures: ● 3D understanding architectures, ● Transformer-based architectures, ● Diffusion-driven frameworks, ● Mamba-based architectures. \* denotes the application of voting strategy. The results of other models are sourced from publicly published papers.

Methods	Reference	Pre-training strategy	ModelNet40 1k P	ScanObjectNN			P (M)	F (G)
				OBJ_BG	OBJ_ONL	PB_T50_RS		
<i>Supervised Learning Only</i>								
<span style="color: red;">●</span> PointNet[4]	CVPR 17	×	89.2	73.3	79.2	68.0	3.5	0.5
<span style="color: red;">●</span> PointNet++[31]	NeurIPS 17	×	90.7	82.3	84.3	77.9	1.5	1.7
<span style="color: red;">●</span> DGCNN[41]	TOG 19	×	92.9	82.8	86.2	78.1	1.8	2.4
<span style="color: red;">●</span> DRNet[33]	WACV-21	×	93.1	-	-	80.3	-	-
<span style="color: red;">●</span> MVTN[15]	ICCV 21	×	93.8	92.6	<b>92.3</b>	82.8	11.2	43.7
<span style="color: red;">●</span> PointMLP[27]	ICLR 22	×	<b>94.5</b>	-	-	85.4±0.3	12.6	31.4
<span style="color: red;">●</span> PointNeXt[32]	NeurIPS 22	×	92.9	-	-	87.7±0.4	1.4	3.6
<span style="color: green;">●</span> Transformer[38]	NeurIPS 17	×	94.1	79.86	80.55	77.24	22.1	4.8
<span style="color: green;">●</span> PointConT[25]	JAS 23	×	93.5	-	-	90.30	-	-
<span style="color: cyan;">●</span> Pointmamba[21]	NeurIPS24	×	-	88.30	87.78	82.48	12.3	3.6
<span style="color: cyan;">●</span> Mamba3D[16]	ACM MM24	×	93.4	92.94	92.08	<b>91.81</b>	16.9	3.9
<span style="color: cyan;">●</span> Hybrid-Emba3D		×	94.0	<b>93.63</b>	92.25	91.05	16.96	3.95
<i>With Self-supervised Pre-training</i>								
<span style="color: green;">●</span> Transformer[38]	NeurIPS 17	OcCo	92.1	84.85	85.54	78.79	22.1	4.8
<span style="color: green;">●</span> MaskPoint[23]	CVPR 22	MaskPoint	93.8	89.30	88.10	84.30	22.1	4.8
<span style="color: green;">●</span> Point-BERT*[48]	CVPR 22	IDPT	93.4	88.12	88.30	83.69	22.1+1.7	4.8
<span style="color: green;">●</span> Point-MAE*[30]	ECCV 22	IDPT	94.4	91.22	90.02	84.94	22.1+1.7	4.8
<span style="color: green;">●</span> PointGPT-S*[5]	NeurIPS 23		94.0	91.6	90.0	86.9	29.2	5.7
<span style="color: green;">●</span> Point-FMAE*[49]	AAAI 24	Point-M2AE	95.15	<b>95.18</b>	93.29	90.22	27.4	3.6
<span style="color: blue;">●</span> PointDif[52]	CVPR 24	PointDif	-	93.29	91.91	87.61	-	-
<span style="color: cyan;">●</span> Pointmamba[21]	NeurIPS 24	Point-MAE	93.6	94.32	92.60	89.31	12.3	3.6
<span style="color: cyan;">●</span> Mamba3D*[16]	ACM MM24	Point-MAE	95.1	<b>95.18</b>	92.60	93.34	16.9	3.9
<span style="color: cyan;">●</span> Hybrid-Emba3D		Point-MAE	<b>95.58+1.58</b>	93.80+0.27	93.12+0.87	93.09+2.04	16.96	3.95
<span style="color: cyan;">●</span> Hybrid-Emba3D*		Point-MAE	<b>95.99+1.99</b>	<b>95.18+1.38</b>	<b>93.80+1.55</b>	<b>94.34+3.29</b>	16.96	3.95

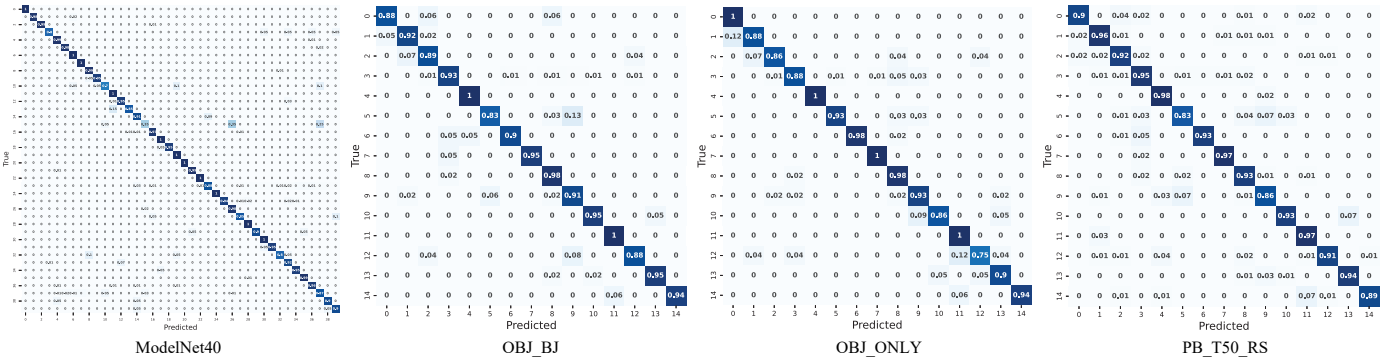


Figure 8: Details of Collaborative feature enhancer

similar geometric structures and overlapping local features result in a specific category-15 (dresser) accuracy of only 35% (consistent with t-SNE), and its confusion rates with category-26 (piano) and category-37 (tv\_stand) are 35% and 25%, respectively.

Comparing OBJ\_ONLY and OBJ\_BG, the presence of background increases the misjudgment rate of locally structurally similar objects. For example, the accuracy of category-0 (bag) decreases from 100% to 88%, and the confusion rate of category-5 (chair) and 9 (shelf) reaches 13%. Conversely, it may also reduce the misclassifications rate caused by fea-

ture overlap, such as the accuracy rate of category-10 and 12 increased from 86% and 75% to 95% and 88%, respectively, and the misjudgment rate of category-9 (shelf) and 10 (table), category-11 (bed) and category-12 (pillow) drops from 9% and 12% to 0%. Under interference (PB\_T50\_RS), the misclassification distribution has shifted, meaning misjudged samples are redistributed among error categories while maintaining a stable overall misjudgment rate.

#### 4.3. Ablation study

To validate the complementary nature and distinct performance boundaries of core components LGP and CoFEBiSSM,

Table 2: Ablation studies on ModelNet40 and ScanObjectNN.

LGP	CoFE-BiSSM	ModelNet40 1k P	ScanObjectNN			P (M)	F (G)
			OBJ_BG	OBJ_ONL	PB_T50_RS		
-	-	93.39	91.60	89.84	90.32	16.93	3.86
✓	-	93.48	92.57	90.88	90.67	16.93	3.86
-	✓	93.56	92.05	90.02	90.49	16.96	3.95
✓	✓	94.00	93.63	92.25	91.05	16.96	3.95

Table 3: The experimental results of ModelNetFewShot. The results of other models are sourced from publicly published papers.

Methods	Reference	5-Way		10-Way	
		10-Shot	20-Shot	10-Shot	20-Shot
<i>Supervised Learning Only</i>					
PointNet[4]	CVPR 17	52.0±3.8	57.8±4.9	46.6±4.3	35.2±4.8
Transformer[38]	NeurIPS 17	87.8±5.2	93.3±4.3	84.6±5.5	89.4±6.3
DGCNN[41]	TOG 19	31.6±2.8	40.8±4.6	19.9±2.1	16.9±1.5
DGCNN+CrossPoint[1]	CVPR 2022	<b>92.5±3.0</b>	94.9±2.1	83.6±5.3	87.9±4.2
Hybrid-Emba3D		90.5±3.8	<b>96.0±3.2</b>	<b>86.3±5.1</b>	<b>92.0±3.4</b>
<i>With Self-supervised Pre-training</i>					
DGCNN+OcCo	NeurIPS 17	90.6±2.8	92.5±1.9	82.9±1.3	86.5±2.2
OcCo[39]	NeurIPS 17	94.0±3.6	95.9±2.7	89.4±5.1	92.4±4.6
ACT[6]	NeurIPS 17	96.8±2.3	98.0±1.4	<b>93.3±4.0</b>	<b>95.6±2.8</b>
MaskPoint[23]	CVPR 22	95.0±3.7	97.2±1.7	91.4±4.0	93.4±3.5
Point-BERT[48]	CVPR 22	94.6±3.1	96.3±2.7	91.0±5.4	92.7±5.1
Point-MAE[30]	ECCV 22	96.3±2.5	97.8±1.8	92.6±4.1	95.0±3.0
PointGPT-S[5]	NeurIPS 23	<b>96.8±2.0</b>	98.6±1.1	92.6±4.6	95.2±3.4
Pointmamba[21]	NeurIPS 24	96.9±2.3	<b>99.0±1.1</b>	93.0±4.0	95.6±2.8
Hybrid-Emba3D		93.3±5.0	98.9±1.3	90.4±5.7	95.6±3.9

across diverse scenarios, we conduct ablation studies on the Hybrid-Emba3D benchmarked on 3D point cloud classification tasks. The results as shown in Table 2

**LGP:** LGP is a core component focusing on local feature extraction. This component captures subtle geometric variations and topological structures on object surfaces by constructing non-linear transformation mechanisms within local neighborhoods. When solely activated, LGP achieves 94.00% accuracy on ModelNet40, demonstrating its strong geometric feature representation in ideal, background-free scenarios. Furthermore, it achieves accuracy gains of +0.97% (OBJ\_BG), +1.04% (OBJ\_ONLY), and +0.35% (PB\_T50\_RS) compared to the deactivated baseline, further validating its capability to resist background clutter and minor deformations through local geometric modeling. It is commendable that it introduces zero additional parameters (0M) and computational costs (0G FLOPs), highlighting superior lightweight design advantages.

**CoFE-BiSSM:** CoFE-BiSSM enhances long-range dependencies through multi-scale feature fusion and bidirectional modeling. It achieves 92.05% accuracy on OBJ\_BG, slightly below LGP’s 92.57%, but with excellent efficiency (0.03M Parameters/0.09G FLOPs). In the ModelNet40 (93.56%) and OBJ\_ONLY (90.02%) scenarios without background interference, the performance is relatively limited, while the rotation disturbance sensitivity on PB\_T50\_RS (90.32%) reveals insuffi-

cient local geometric modeling. Experiments demonstrate its effectiveness in global context reasoning for complex background tasks, but it requires integration with local feature extraction modules to address geometric sensitivity.

**Joint effect:** Component collaboration yields significant performance gains. At the peak of 94.00% (+0.61%) in ModelNet40, all subsets of ScanObjectNN surpassed the single component configuration comprehensively, with OBJ\_BG improving by 2.03%, OBJ\_ONLY improving by 2.41%, and PB\_T50\_RS improving by 0.73%. They achieve feature complementarity with minimal overhead. In summary, LGP and CoFE-BiSSM focus on local geometric and global multi-scale modeling, respectively. While their strengths are scenario-specific, joint deployment enables complementary features and enhances generalization performance on different datasets.

#### 4.4. Few-shot Learning

**Datasets and Settings:** ModelNetFewShot is the ModelNet40-based 3D few-shot benchmark for evaluating classification algorithms’ generalization with limited samples. It adopts N-way K-shot tasks, randomly selecting N classes (K training samples per class) and testing on the remaining instances. Results report mean accuracy ± standard deviation across 10 independent trials. The results are shown in Table 3.

**Results:** Without pretraining, Hybrid-Emba3D achieves 90.5% on 5-Way 10-Shot, surpassing Transformer (87.8±5.2) but lagging behind DGCNN-CrossPoint (92.5%). Scaling to 20-shot boosts accuracy by 6% (96.0%). For 10-Way tasks, it outperforms DGCNN-CrossPoint. With self-supervised pretraining, it is worth noting that Hybrid-Emba3D outperforms PointGPT-S (98.6%) in 5-Way 20 Shot, achieving a quasi SOTA performance of 98.9%. However, the advantage has not been generalized to other settings. In the 5/10-Way task, the accuracy rate increased by 5.6% and 5.2% when the sample size increased from 10-Shot to 20-Shot, and the standard deviation dropped sharply by 74% and 32%, indicating that the model is sensitive to data sparsity, and data enhancement can significantly improve performance and stability.

## 5. Conclusion

In this paper, we present Hybrid-Emba3D, a novel mamba-based Architecture for point cloud classification task, designing two key components: the geometry-feature coupling mechanism that aggregates geometric information from neighboring points around each centroid and central feature to enhance local geometric representation, and A multidimensional feature hybrid enhancer employing dual-path Architecture to strengthen global context modeling for BiSSM. Notably, the total computational cost with the two components is very small. Especially in the operations of coupling local geometric information into central features in a parameter-free manner, incurring no additional parameters, that is completely driven by local neighborhoods' intrinsic geometric relationships.

Extensive experiments demonstrate Hybrid-Emba3D's superior performance across classification benchmarks, particularly achieving new SOTA accuracy on ModelNet40 at the cost of minimal parameters. These also show that the Mamba architecture has potential, yet insufficient exploration in point cloud processing.

## References

- [1] Mohamed Afham, Isuru Dissanayake, Dinithi Dissanayake, Amaya Dharmasiri, Kanchana Thilakarathna, and Ranga Rodrigo. Crosspoint: Self-supervised cross-modal contrastive learning for 3d point cloud understanding. In *2022 IEEE/CVF Conference on Computer Vision and Pattern Recognition (CVPR)*, pages 9892–9902, 2022.
- [2] Tamer Basar. *A New Approach to Linear Filtering and Prediction Problems*, pages 167–179. Wiley-IEEE Press, 2001.
- [3] Angel X. Chang, Thomas A. Funkhouser, Leonidas J. Guibas, Pat Hanrahan, Qi-Xing Huang, Zimo Li, Silvio Savarese, Manolis Savva, Shuran Song, Hao Su, Jianxiong Xiao, Li Yi, and Fisher Yu. Shapenet: An information-rich 3d model repository. *CoRR*, abs/1512.03012, 2015.
- [4] R. Q. Charles, H. Su, M. Kaichun, and L. J. Guibas. Pointnet: Deep learning on point sets for 3d classification and segmentation. In *2017 IEEE Conference on Computer Vision and Pattern Recognition (CVPR)*, pages 77–85, 2017.
- [5] Guangyan Chen, Meiling Wang, Yi Yang, Kai Yu, Li Yuan, and Yufeng Yue. Pointgpt: Auto-regressively generative pre-training from point clouds, 2023.
- [6] Runpei Dong, Zekun Qi, Linfeng Zhang, Junbo Zhang, Jianjian Sun, Zheng Ge, Li Yi, and Kaisheng Ma. Autoencoders as cross-modal teachers: Can pretrained 2d image transformers help 3d representation learning?, 2023.
- [7] Alexey Dosovitskiy, Lucas Beyer, Alexander Kolesnikov, Dirk Weissenborn, Xiaohua Zhai, Thomas Unterthiner, Mostafa Dehghani, Matthias Minderer, Georg Heigold, Sylvain Gelly, Jakob Uszkoreit, and Neil Houlsby. An image is worth 16x16 words: Transformers for image recognition at scale. *CoRR*, abs/2010.11929, 2020.
- [8] N. Engel, V. Belagiannis, and K. Dietmayer. Point transformer. *IEEE Access*, 9:134826–134840, 2021.
- [9] Francis Engelmann, Theodora Kontogianni, and Bastian Leibe. Dilated point convolutions: On the receptive field size of point convolutions on 3d point clouds. In *2020 IEEE International Conference on Robotics and Automation (ICRA)*, pages 9463–9469, 2020.
- [10] Lue Fan, Ziqi Pang, Tianyuan Zhang, Yu-Xiong Wang, Hang Zhao, Feng Wang, Naiyan Wang, and Zhaoxiang Zhang. Embracing single stride 3d object detector with sparse transformer. In *2022 IEEE/CVF Conference on Computer Vision and Pattern Recognition (CVPR)*, pages 8448–8458, 2022.
- [11] Albert Gu and Tri Dao. Mamba: Linear-time sequence modeling with selective state spaces, 2024.
- [12] Albert Gu, Karan Goel, and Christopher Ré. Efficiently modeling long sequences with structured state spaces. In *The Tenth International Conference on Learning Representations, ICLR 2022, Virtual Event, April 25–29, 2022*, 2022.
- [13] Albert Gu, Isys Johnson, Karan Goel, Khaled Saab, Tri Dao, Atri Rudra, and Christopher Ré. Combining recurrent, convolutional, and continuous-time models with linear state-space layers, 2021.
- [14] Meng-Hao Guo, Jun-Xiong Cai, Zheng-Ning Liu, Tai-Jiang Mu, Ralph R. Martin, and Shi-Min Hu. Pct: Point cloud transformer. *Computational Visual Media*, 7(2):187–199–187–199, 2021.
- [15] Abdullah Hamdi, Silvio Giancola, and Bernard Ghanem. Mvtn: Multi-view transformation network for 3d shape recognition, 2021.
- [16] Xu Han, Yuan Tang, Zhaoxuan Wang, and Xianzhi Li. Mamba3d: Enhancing local features for 3d point cloud analysis via state space model. In *Proceedings of the 32nd ACM International Conference on Multimedia, MM 2024, Melbourne, VIC, Australia, 28 October 2024 - 1 November 2024*, pages 4995–5004. ACM, 2024.
- [17] Roman Klokov and Victor Lempitsky. Escape from cells: Deep kd-networks for the recognition of 3d point cloud models. In *2017 IEEE International Conference on Computer Vision (ICCV)*, pages 863–872, 2017.
- [18] Xuemei Li, Min Li, Bin Liu, Shangsong Lv, and Chengjie Liu. A novel transformer network based on cross-spatial learning and deformable attention for composite fault diagnosis of agricultural machinery bearings. *Agriculture-Basel*, 14(8):1397, 2024.
- [19] Xuemei Li, Bin Liu, Shangsong Lv, Min Li, and Chengjie Liu. A fast registration method for mems lidar point cloud based on self-adaptive segmentation. *Electronics*, 12(19):4006, 2023.
- [20] Yangyan Li, Rui Bu, Mingchao Sun, Wei Wu, Xinhan Di, and Baoquan Chen. Pointcnn: convolution on  $X$ -transformed points. In *Proceedings of the 32nd International Conference on Neural Information Processing Systems*, page 828–838, Red Hook, NY, USA, 2018. Curran Associates Inc.
- [21] Dingkan Liang, Xin Zhou, Wei Xu, Xinghui Zhu, Zhikang Zou, Xiaojing Ye, Xiao Tan, and Xiang Bai. Pointmamba: A simple state space model for point cloud analysis. In *Advances in Neural Information Processing Systems*, volume 37, pages 32653–32677. Curran Associates, Inc., 2024.
- [22] Zachary C. Lipton, John Berkowitz, and Charles Elkan. A critical review of recurrent neural networks for sequence learning, 05 2015.
- [23] Haotian Liu, Mu Cai, and Yong Jae Lee. Masked discrimination for self-supervised learning on point clouds. In *Computer Vision – ECCV 2022*, pages 657–675, Cham, 2022.
- [24] Xuan Liu, Yumo Zhang, Runmin Cong, Chen Zhang, Ning Yang, Chunjie Zhang, and Yao Zhao. Grgnet: Global graph reasoning network for salient object detection in optical remote sensing images. In *Pattern Recognition and Computer Vision: 4th Chinese Conference, PRCV 2021, Beijing, China, October 29 – November 1, 2021, Proceedings, Part II*, page 584–596, Berlin, Heidelberg, 2021. Springer-Verlag.
- [25] Yahui Liu, Bin Tian, Yisheng Lv, Lingxi Li, and Fei-Yue Wang. Point cloud classification using content-based transformer via clustering in feature space. *IEEE/CAA Journal of Automatica Sinica*, 11(1):231, 2024.
- [26] Yongcheng Liu, Bin Fan, Shiming Xiang, and Chunhong Pan. Relation-

- shape convolutional neural network for point cloud analysis. In *2019 IEEE/CVF Conference on Computer Vision and Pattern Recognition (CVPR)*, pages 8887–8896, 2019.
- [27] Xu Ma, Can Qin, Haoxuan You, Haoxi Ran, and Yun Fu. Rethinking network design and local geometry in point cloud: A simple residual mlp framework, 2022.
- [28] Y. Ma, Y. Guo, H. Liu, Y. Lei, and G. Wen. Global context reasoning for semantic segmentation of 3d point clouds. In *2020 IEEE Winter Conference on Applications of Computer Vision (WACV)*, pages 2920–2929, 2020.
- [29] Daniel Maturana and Sebastian Scherer. Voxnet: A 3d convolutional neural network for real-time object recognition. In *2015 IEEE/RSJ International Conference on Intelligent Robots and Systems (IROS)*, pages 922–928, 2015.
- [30] Yatian Pang, Wenxiao Wang, Francis E. H. Tay, Wei Liu, Yonghong Tian, and Li Yuan. Masked autoencoders for point cloud self-supervised learning. In *Computer Vision – ECCV 2022*, pages 604–621, Cham, 2022. Springer Nature Switzerland.
- [31] Charles R. Qi, Li Yi, Hao Su, and Leonidas J. Guibas. Pointnet++: deep hierarchical feature learning on point sets in a metric space. In *Proceedings of the 31st International Conference on Neural Information Processing Systems, NIPS’17*, page 5105–5114, Red Hook, NY, USA, 2017. Curran Associates Inc.
- [32] Guocheng Qian, Yuchen Li, Houwen Peng, Jinjie Mai, Hasan Hammoud, Mohamed Elhoseiny, and Bernard Ghanem. Pointnext: Revisiting pointnet++ with improved training and scaling strategies. In *Neural Information Processing Systems*, volume 35, pages 23192–23204, 2022.
- [33] Shi Qiu, Saeed Anwar, and Nick Barnes. Dense-resolution network for point cloud classification and segmentation. In *2021 IEEE Winter Conference on Applications of Computer Vision (WACV)*, pages 3812–3821, 2021.
- [34] Gernot Riegler, Ali Osman Ulusoy, and Andreas Geiger. Octnet: Learning deep 3d representations at high resolutions. In *2017 IEEE Conference on Computer Vision and Pattern Recognition (CVPR)*, pages 6620–6629, 2017.
- [35] Peize Sun, Rufeng Zhang, Yi Jiang, Tao Kong, Chenfeng Xu, Wei Zhan, Masayoshi Tomizuka, Lei Li, Zehuan Yuan, Changhu Wang, and Ping Luo. Sparse r-cnn: End-to-end object detection with learnable proposals. In *2021 IEEE/CVF Conference on Computer Vision and Pattern Recognition (CVPR)*, pages 14449–14458, 2021.
- [36] Hugues Thomas, Charles R. Qi, Jean-Emmanuel Deschaud, Beatriz Marcotequi, François Goulette, and Leonidas Guibas. Kpconv: Flexible and deformable convolution for point clouds. In *2019 IEEE/CVF International Conference on Computer Vision (ICCV)*, pages 6410–6419, 2019.
- [37] Mikaela Angelina Uy, Quang-Hieu Pham, Binh-Son Hua, Thanh Nguyen, and Sai-Kit Yeung. Revisiting point cloud classification: A new benchmark dataset and classification model on real-world data. In *2019 IEEE/CVF International Conference on Computer Vision (ICCV)*, pages 1588–1597, 2019.
- [38] Ashish Vaswani, Noam Shazeer, Niki Parmar, Jakob Uszkoreit, Llion Jones, Aidan N. Gomez, Lukasz Kaiser, and Illia Polosukhin. Attention is all you need. In *Proceedings of the 31st International Conference on Neural Information Processing Systems, NIPS’17*, page 6000–6010, Red Hook, NY, USA, 2017. Curran Associates Inc.
- [39] H. Wang, Q. Liu, X. Yue, J. Lasenby, and M. J. Kusner. Unsupervised point cloud pre-training via occlusion completion. In *2021 IEEE/CVF International Conference on Computer Vision (ICCV)*, pages 9762–9772, 2021.
- [40] L. Wang, Y. Huang, Y. Hou, S. Zhang, and J. Shan. Graph attention convolution for point cloud semantic segmentation. In *2019 IEEE/CVF Conference on Computer Vision and Pattern Recognition (CVPR)*, pages 10288–10297, 2019.
- [41] Yue Wang, Yongbin Sun, Ziwei Liu, Sanjay E. Sarma, Michael M. Bronstein, and Justin M. Solomon. Dynamic graph cnn for learning on point clouds. *ACM Trans. Graph.*, 38(5), October 2019.
- [42] Yufan Wang, Qunfei Zhao, and Zeyang Xia. Multi-guided feature refinement for point cloud semantic segmentation with weakly supervision. *Knowledge-Based Systems*, 311:113050, 2025.
- [43] Hangbin Wu, Zerán Xu, Chun Liu, Akram Akbar, Han Yue, Doudou Zeng, and Huimin Yang. Lv-gcnn: A lossless voxelization integrated graph convolutional neural network for surface reconstruction from point clouds. *International Journal of Applied Earth Observation and Geoinformation*, 103:102504, 2021.
- [44] Wenxuan Wu, Zhongang Qi, and Li Fuxin. Pointconv: Deep convolutional networks on 3d point clouds. In *2019 IEEE/CVF Conference on Computer Vision and Pattern Recognition (CVPR)*, pages 9613–9622, 2019.
- [45] Xiaoyang Wu, Li Jiang, Peng-Shuai Wang, Zhijian Liu, Xihui Liu, Yu Qiao, Wanli Ouyang, Tong He, and Hengshuang Zhao. Point transformer v3: Simpler, faster, stronger. In *2024 IEEE/CVF Conference on Computer Vision and Pattern Recognition (CVPR)*, pages 4840–4851, 2024.
- [46] Zhirong Wu, Shuran Song, Aditya Khosla, Fisher Yu, Linguang Zhang, Xiaoou Tang, and Jianxiong Xiao. 3d shapenets: A deep representation for volumetric shapes. In *2015 IEEE Conference on Computer Vision and Pattern Recognition (CVPR)*, pages 1912–1920, 2015.
- [47] Yifan Xu, Tianqi Fan, Mingye Xu, Long Zeng, and Yu Qiao. Spidercnn: Deep learning on point sets with parameterized convolutional filters. In Vittorio Ferrari, Martial Hebert, Cristian Sminchisescu, and Yair Weiss, editors, *Computer Vision – ECCV 2018*, pages 90–105, Cham, 2018. Springer International Publishing.
- [48] Xumin Yu, Lulu Tang, Yongming Rao, Tiejun Huang, Jie Zhou, and Jiwen Lu. Point-bert: Pre-training 3d point cloud transformers with masked point modeling. In *2022 IEEE/CVF Conference on Computer Vision and Pattern Recognition (CVPR)*, pages 19291–19300, 2022.
- [49] Yaohua Zha, Huizhen Ji, Jinmin Li, Rongsheng Li, Tao Dai, Bin Chen, Zhi Wang, and Shu-Tao Xia. Towards compact 3d representations via point feature enhancement masked autoencoders. In *Proceedings of the Thirty-Eighth AAAI Conference on Artificial Intelligence and Thirty-Sixth Conference on Innovative Applications of Artificial Intelligence and Fourteenth Symposium on Educational Advances in Artificial Intelligence, AAAI’24/IAAI’24/EAAI’24*. AAAI Press, 2024.
- [50] Cheng Zhang, Haocheng Wan, Xinyi Shen, and Zizhao Wu. Patchformer: An efficient point transformer with patch attention. In *2022 IEEE/CVF Conference on Computer Vision and Pattern Recognition (CVPR)*, pages 11789–11798, 2022.
- [51] Xindan Zhang, Ying Li, and Xinnian Zhang. Asmpw: Adaptive spatial masking for weakly-supervised point cloud semantic segmentation. *Knowledge-Based Systems*, 310:113016, 2025.
- [52] Xiao Zheng, Xiaoshui Huang, Guofeng Mei, Yuenan Hou, Zhaoyang Lyu, Bo Dai, Wanli Ouyang, and Yongshun Gong. Point cloud pre-training with diffusion models. In *2024 IEEE/CVF Conference on Computer Vision and Pattern Recognition (CVPR)*, pages 22935–22945, 2024.
- [53] Lianghui Zhu, Bencheng Liao, Qian Zhang, Xinlong Wang, Wenyu Liu, and Xinggang Wang. Vision mamba: Efficient visual representation learning with bidirectional state space model. In *41st International Conference on Machine Learning*, 2024.